Frozen-Orbital Analysis of the Excited States of Metal Complexes in High Symmetry: Oh Case

ARTICLE *in* THE JOURNAL OF PHYSICAL CHEMISTRY · SEPTEMBER 1996

Impact Factor: 2.78 · DOI: 10.1021/jp960310x

3 AUTHORS, INCLUDING:

Hiromi Nakai
Waseda University
221 PUBLICATIONS **3,218** CITATIONS

SEE PROFILE

Frozen-Orbital Analysis of the Excited States of Metal Complexes in High Symmetry: O_h Case

Hiromi Nakai,[†,‡] Hiroshi Morita,[†] and Hiroshi Nakatsuji*[,†,§]

Department of Synthetic Chemistry and Biological Chemistry, Faculty of Engineering, Kyoto University, Sakyo-ku, Kyoto 606-01, Japan, and Institute for Fundamental Chemistry, 34-4, Takano-Nishihiraki-cho, Sakyo-ku, Kyoto 606, Japan

Received: January 31, 1996; In Final Form: May 18, 1996[⊗]

A frozen-orbital analysis (FZOA) is proposed in order to understand the nature and the ordering of the excited states due to the excitations between degenerate orbitals of metal complexes in high symmetry. The FZOA method represents a direct application of group theory. In the FZOA approach, only a few two-electron integrals are considered to explain the ordering and the energy splittings of the excited states, which are brought about by excitations between two degenerate orbitals. Furthermore, FZOA may be utilized to explain the intensities of the absorption peaks. Here, we apply FZOA to two series of the excited states of MoF_6. Although there are large discrepancies between the actual excitation energies by FZOA and those derived by more accurate calculations, the ordering and the energy splittings are comparable. This relative agreement is sufficient to justify an analysis based on FZOA methods. On the basis of the present results, we suggest that FZOA methods would yield some general insight into the nature of the excited states for molecules of high symmetry.

I. Introduction

Transition metal complexes are characterized by a variety of absorption spectra in the visible and UV regions. Extensive experimental studies of their electronic spectra have been undertaken.[1] These results essentially give us information about the electronic excited states corresponding to dipole-allowed transitions. Some of the data on the absorption of metal complex ions in crystalline fields indicate the existence of several excited states to which dipole transitions are forbidden in the absence of perturbation. For example, although the lowest transition of $^1T_1$ symmetry is forbidden for the tetrahedral permanganate ion MnO_4^- in solution,[2] the corresponding transitions are observed in the lithium and barium salts, $LiMnO_4 \cdot 3H_2O$ (C_{3v}) and $Ba(MnO_4)_2 \cdot 3H_2O$ (C_3).[3] Most photochemical reactions of metal complexes, which are often important as homogeneous photocatalytic reactions, involve both allowed and forbidden excited states.[4−6] Here, a more systematic understanding of the nature of all of these excited states is essential in designing photochemical reactions.

Theoretical studies have played important roles in clarifying the excited states of metal complexes. Early theoretical approaches were based on the empirical or semiempirical method, which used experimental values as parameters. The ligand field theory (LFT) was developed by combining crystal field theory with molecular orbital (MO) theory.[7−10] In LFT, the energy levels of the ligand field absorption bands are estimated with parameters such as Dq, B, and C, which are inherent in Orgel diagrams[11] or Tanabe−Sugano diagrams.[12] An extension of LFT to strong bands, which are caused by electron transfer between the metal and its ligands, was presented by Jørgensen.[10,13] Wolfsberg and Helmholtz applied a semiempirical MO theory to the inorganic complex ions CrO_4^{2-}, MnO_4^-, and ClO_4^-.[14] The group overlap integrals obtained with the σ and π metal−ligand overlaps were used to estimate the energy levels of the excited states. However, while of great historical significance, these pioneering approaches do not necessarily give reliable results due to the use of many parameters.

The Xα method and ab initio MO methods, such as configuration interaction (CI) calculations, have also been used to examine the assignments for the absorption bands. These methods do not use parameters. However, without the adequate inclusion of electron correlations, the calculated excitation energies do not agree well with experimental values, and as a consequence, several different assignments are proposed.

On the other hand, the accuracy of the symmetry adapted cluster (SAC)[15]/SAC-CI[16] method has been confirmed by application to many organic and inorganic systems.[17] For example, the agreement between the SAC/SAC-CI and full-CI methods has been verified for small molecules.[18] The SAC/SAC-CI calculations for several metal complexes, such as MO_4^{q-} (M = Ru, Os, Mn, Tc, Cr, Mo; q = 0∼2),[19−23] $MoO_{4-n}S_n^{2-}$ (n = 0∼4),[23] TiL_4 (L = Cl, Br, I),[24,25] CrO_2Cl_2,[26] and SnL_4 (L = H and CH_3),[27] have given reasonable and reliable assignments for experimental absorption peaks. Also, the range of systems to which the SAC/SAC-CI method can be applied now has increased because of improvements both in computational resources and in the nature of computational algorithms. We have recently applied the SAC-CI method for studying the excitation spectra of porphyrins; including free-base porphin,[28] Mg-porphin,[29] oxyheme,[30] tetrazaporphin,[31] etc.

Recently, Roos and co-workers presented the CASPT2 method.[32,33] This is a second-order perturbation theory which uses complete-active-space self-consistent-field (CASSCF) wave functions. Their method has given reliable results.[34,35]

We are now at a point where we can develop a general rule and concept regarding the excited states of metal complexes based on these accurate results. However, electron correlations, which are essential for accurate descriptions, as mentioned above, are different in excited states even for the same

† Kyoto University.
‡ Present address: Department of Chemistry, School of Science and Engineering, Waseda University, Tokyo 169, Japan.
§ Institute for Fundamental Chemistry.
⊗ Abstract published in *Advance ACS Abstracts,* September 1, 1996.

S0022-3654(96)00310-3 CCC: $12.00

complexes. Therefore, it is difficult to explain theoretical results using such correlation effects alone.

In this report, we propose a frozen-orbital analysis (FZOA) to explain the ordering and the splitting of excited states of identical term-multiplicity. We report here a preliminary result of the application of FZOA to two series of the excited states ($7t_{1u} \rightarrow 3t_{2g}$ and $6t_{1u} \rightarrow 3t_{2g}$) of octahedral MoF_6. Despite some large discrepancies between the excitation energies in FZOA and SAC-CI calculations, the energy ordering and the splitting are comparable by the two methods. The origin of the different orderings of the $7t_{1u} \rightarrow 3t_{2g}$ and $6t_{1u} \rightarrow 3t_{2g}$ excited states is clarified by the present analysis. Furthermore, FZOA may be used to explain also the strengths of the two peaks due to $7t_{1u} \rightarrow 3t_{2g}$ and $6t_{1u} \rightarrow 3t_{2g}$ excitations. In conclusion, we give a general rule for the excited states of the two $t_{1u} \rightarrow t_{2g}$ excitations of octahedral metal complexes.

II. Principle of Frozen-Orbital Analysis (FZOA)

We present here an expression for the excitation energies between degenerate MOs based on the FZO approximation, which corresponds to a first-order perturbation treatment with the use of Hartree–Fock (HF) wave function. In comparison, we first show the singlet and triplet excitation energies between nondegenerate MOs by the FZO approximation and discuss them in terms of Hund's rule.[36] Next, to explain the ordering and the splitting of the excited states between the same degenerate MOs, we present the methodology of FZOA, in which the various two-electron integrals in the energy expressions are analyzed using the densities and transition densities.

In the first-order perturbation treatment, the singlet and triplet excitation energies $^1\Delta E$ and $^3\Delta E$ of the transitions from a nondegenerate ith MO ϕ_i to another nondegenerate ath MO ϕ_a are represented by

$$^1\Delta E = (\epsilon_a - \epsilon_i) + (-J_{ia} + 2K_{ia}) \quad (1)$$

$$^3\Delta E = (\epsilon_a - \epsilon_i) + (-J_{ia}) \quad (2)$$

where ϵ is the orbital energy and J and K are Coulomb and exchange integrals, respectively. On comparing eqs 1 and 2, one notes that the energy difference between the singlet and triplet states falls by $2K_{ia}$. Since $K > 0$, we immediately obtain the correct sign for the energy splitting. This explains Hund's rule of maximum multiplicity in which, for a given electronic configuration, the state with the highest multiplicity has the lowest energy.[36] This explanation for singlet–triplet separation is generally accepted in many texts on quantum mechanics. However, in fact, the difference is negative when it is evaluated with accurate wave functions. Many theoretical studies have tried to clarify the reasons for this discrepancy.[37–48]

According to the study on He by Kohl,[40] the electron–electron repulsion energy for the same pair of spatial orbitals, which is smaller for the triplet than for the singlet, is not the dominant contribution to the total energy. In the transition from the first-order perturbation treatment to the exact solution, the redistribution of charge results in a substantial lowering of the nuclear attraction term in the triplet, which determines the energy levels of the singlet and triplet states. Nevertheless, we think that a discussion of the first-order perturbation treatment is important.

Next, we discuss systems with higher symmetries, such as O_h and T_d. We consider O_h as an example. The present discussion can be easily extended to other symmetries. In general, octahedral metal complexes have six σ-character MOs, a_{1g}, e_g, and t_{1u}, and 12 π-character MOs, t_{1g}, t_{2g}, t_{1u}, and t_{2u}, all of which consist of the p orbitals of the ligands. The d orbitals of the metal are split into t_{2g} and e_g MOs by the octahedral ligand field. For d^0 complexes such as MoF_6, the valence excited states in the UV–visible region have the nature of one-electron excitations to the t_{2g} MOs of the metal d orbitals. On the other hand, one-electron excitations from the t_{2g} MOs are seen in the valence excited states of d^6 complexes such as $Mo(CO)_6$. These statements are verified by SAC/SAC-CI calculations in the present and separate studies.[49,50] The symmetries of the lower excited states, therefore, correspond to the right-hand side of the following equations of direct-product decomposition:

$$a_{1g} \times t_{2g} = t_{2g} \quad (3)$$

$$e_g \times t_{2g} = t_{1g} + t_{2g} \quad (4)$$

$$t_{1g} \times t_{2g} = a_{2g} + e_g + t_{1g} + t_{2g} \quad (5)$$

$$t_{2g} \times t_{2g} = a_{1g} + e_g + t_{1g} + t_{2g} \quad (6)$$

$$t_{1u} \times t_{2g} = a_{2u} + e_u + t_{1u} + t_{2u} \quad (7)$$

$$t_{2u} \times t_{2g} = a_{1u} + e_u + t_{1u} + t_{2u} \quad (8)$$

In the cases of eqs 4–8, which correspond to the excitations between degenerate MOs and give plural excited states, eqs 1 and 2 are not applicable and do not explain the splittings among the excited states.

Excitation from t_{1u} to t_{2g} can be considered as an example. When three ϕ_i, ϕ_j, and ϕ_k MOs of t_{1u} symmetry are assigned to b_{1u} (z), b_{2u} (y), and b_{3u} (x) elements of D_{2h} symmetry, respectively, and ϕ_a, ϕ_b, and ϕ_c MOs of t_{2g} symmetry are assigned to b_{1g} (xy), b_{2g} (zx), and b_{3g} (yz) elements, respectively, single excitations from (ϕ_i, ϕ_j, and ϕ_k) to (ϕ_a, ϕ_b, and ϕ_c) can be mapped onto three categories of irreducible representations of D_{2h}:

$$A_u: \quad \phi_i \rightarrow \phi_a, \quad \phi_j \rightarrow \phi_b, \quad \phi_k \rightarrow \phi_c \quad (9)$$

$$B_{1u}: \quad \phi_j \rightarrow \phi_c, \quad \phi_k \rightarrow \phi_b \quad (10)$$

$$B_{2u}: \quad \phi_k \rightarrow \phi_a, \quad \phi_i \rightarrow \phi_c \quad (11)$$

$$B_{3u}: \quad \phi_i \rightarrow \phi_b, \quad \phi_j \rightarrow \phi_a \quad (12)$$

The four distinct states on the right-hand side of eq 7 give rise to the following wave functions:

$$A_{2u}: \quad \Psi(A_u) = (1/\sqrt{3})(\Phi_i^a + \Phi_j^b + \Phi_k^c) \quad (13)$$

$$E_u: \quad \Psi(A_u) = (1/\sqrt{2})(\Phi_i^a - \Phi_j^b) \quad (14)$$

$$\Psi(A_u) = (1/\sqrt{6})(\Phi_i^a + \Phi_j^b - 2\Phi_k^c) \quad (15)$$

$$T_{1u}: \quad \Psi(B_{1u}) = (1/\sqrt{2})(\Phi_j^c + \Phi_k^b) \quad (16)$$

$$\Psi(B_{2u}) = (1/\sqrt{2})(\Phi_k^a + \Phi_i^c) \quad (17)$$

$$\Psi(B_{3u}) = (1/\sqrt{2})(\Phi_i^b + \Phi_j^a) \quad (18)$$

$$T_{2u}: \quad \Psi(B_{1u}) = (1/\sqrt{2})(\Phi_j^c - \Phi_k^b) \quad (19)$$

$$\Psi(B_{2u}) = (1/\sqrt{2})(\Phi_k^a - \Phi_i^c) \quad (20)$$

$$\Psi(B_{3u}) = (1/\sqrt{2})(\Phi_i^b - \Phi_j^a) \quad (21)$$

where Φ_i^a is the symmetry-adapted configuration state function of the single excitation from ϕ_i to ϕ_a. In the FZO approximation, the singlet excitation energies are calculated to be

$$^1\Delta E(A_{2u}) = (\epsilon_a - \epsilon_i) + (-J_{ia} + 2K_{ia}) + 2\{2(ai|jb) - (ab|ij)\} \quad (22)$$

$$^1\Delta E(E_u) = (\epsilon_a - \epsilon_i) + (-J_{ia} + 2K_{ia}) - \{2(ai|jb) - (ab|ij)\} \quad (23)$$

$$^1\Delta E(T_{1u}) = (\epsilon_a - \epsilon_i) + (-J_{ja} + 2K_{ja}) + \{2(aj|ib) - (ab|ij)\} \quad (24)$$

$$^1\Delta E(T_{2u}) = (\epsilon_a - \epsilon_i) + (-J_{ja} + 2K_{ja}) - \{2(aj|ib) - (ab|ij)\} \quad (25)$$

where $(ai|jb)$, $(aj|ib)$, and $(ab|ij)$ are four-center two-electron integrals. To derive eqs 22−25, we use the symmetric rule for the integrals; for example, $\epsilon_a = \epsilon_b = \epsilon_c$, $J_{ia} = J_{jb} = J_{kc}$, $(ab|ij) = (bc|jk) = (ca|ki)$, etc. Note that the values of J_{ia} and J_{ja} and also those of K_{ia} and K_{ja} are different, despite the use of the symmetric rule. As in the singlet case, the triplet excitation energies are represented by

$$^3\Delta E(A_{2u}) = (\epsilon_a - \epsilon_i) + (-J_{ia}) - 2(ab|ij) \quad (26)$$

$$^3\Delta E(E_u) = (\epsilon_a - \epsilon_i) + (-J_{ia}) + (ab|ij) \quad (27)$$

$$^3\Delta E(T_{1u}) = (\epsilon_a - \epsilon_i) + (-J_{ja}) - (ab|ij) \quad (28)$$

$$^3\Delta E(T_{2u}) = (\epsilon_a - \epsilon_i) + (-J_{ja}) + (ab|ij) \quad (29)$$

These energy expressions in eqs 22−29 are derived directly using group theory, as indicated above. Similar expressions were presented in a semiempirical MO study by Wolfsberg and Helmholtz.[14] The semiempirical MO method used these expressions for parametrization, i.e., the integrals in the equations were estimated from known experimental values and the excitation energies were calculated using these parameters. On the other hand, the use of energy expressions here is quite different from that in the previous study. Now we are able to obtain accurate solutions by ab initio MO methods that adequately include the correlation effects. Therefore, we use eqs 22−29 to understand the ordering and the splitting of the excited states, as calculated by the more accurate method.

The right-hand sides of eqs 22−29 can be divided into three parts:

$$\Delta E = A + B + C \quad (30)$$

where A is the orbital energy difference, B is the $(-J + 2K)$ or $(-J)$ term, and C is the remaining term. Figure 1 shows a schematic illustration of the energy splitting of the four singlet excited states of $t_{1u} \rightarrow t_{2g}$. The energy level on the left-hand side of Figure 1 is the contribution of the A term, which does not produce energy splitting for excitations between the degenerate MOs. The two energy levels in the middle are due to the B term, which produces energy splitting between ($^1A_{2u}$, ^1E_u) and ($^1T_{1u}$, $^1T_{2u}$). The four energy levels on the right-hand side are due to the C term, which produces further energy splittings between $^1A_{2u}$ and ^1E_u and between $^1T_{1u}$ and $^1T_{2u}$.

Analysis of two-electron integrals such as J_{ia}, J_{ja}, K_{ia}, K_{ja}, $(ai|jb)$, $(aj|ib)$, and $(ab|ij)$ is important for an understanding of the above energy splittings. The spatial distributions of the electron densities $\phi_j^*(r)\phi_j(r)$ and $\phi_a^*(r)\phi_a(r)$ are associated with J_{ja}, i.e., the integral decreases as the distance between the electron densities increases. For both K_{ja} and $(aj|ib)$, the transition density or the overlap between the two molecular orbitals, $\phi_a^*(r)\phi_j(r)$, provides a large contribution. The difference between the maxima of transition densities of $\phi_a^*(r)\phi_j(r)$ and $\phi_i^*(r)\phi_b(r)$ is also important for $(aj|ib)$. Of course, the integrals $\int\phi_a^*(r)\phi_j(r)\,dr$ and $\int\phi_i^*(r)\phi_b(r)\,dr$ both vanish due to the orthogonality of the MOs.

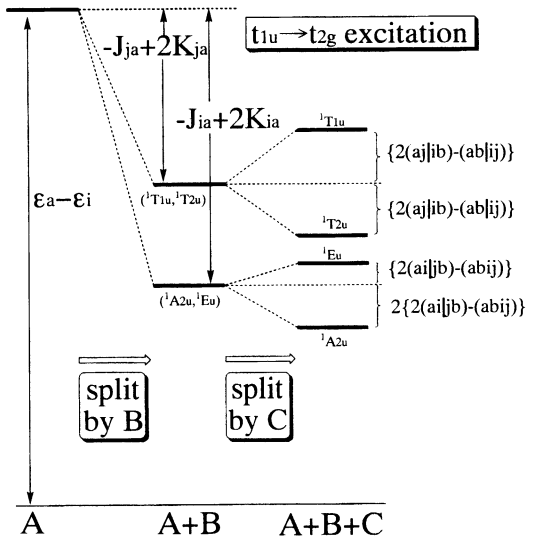

Figure 1. Illustration of the energy splitting of the four singlet excited states, $^1A_{2u}$, ^1E_u, $^1T_{1u}$, and $^1T_{2u}$, of the $t_{1u} \rightarrow t_{2g}$ excitation. The splitting between ($^1A_{2u}$, ^1E_u) and ($^1T_{1u}$, $^1T_{2u}$) is due to the B term in eq 30. Further splitting between $^1A_{2u}$ and ^1E_u and between $^1T_{1u}$ and $^1T_{2u}$ is due to the C term.

The intensities of the absorption bands are calculated by using the square of the transition dipole moment. The transition dipole moments for the four states of $t_{1u} \rightarrow t_{2g}$ are calculated as follows:

$$\langle\Psi(^1A_{2u})|r|\Phi_0\rangle = (1/\sqrt{3})(\langle\Phi_0|r|\Phi_i^a\rangle + \langle\Phi_0|r|\Phi_j^b\rangle + \langle\Phi_0|r|\Phi_k^c\rangle) = 0 \quad (31)$$

$$\langle\Psi(^1E_u)|r|\Phi_0\rangle = (1/\sqrt{2})(\langle\Phi_0|r|\Phi_i^a\rangle - \langle\Phi_0|r|\Phi_j^b\rangle) = 0 \quad (32)$$

$$\langle\Psi(^1T_{1u})|r|\Phi_0\rangle = (1/\sqrt{2})(\langle\Phi_0|r|\Phi_j^c\rangle + \langle\Phi_0|r|\Phi_k^b\rangle) = \sqrt{2}\langle\phi_a|r|\phi_j\rangle \quad (33)$$

$$\langle\Psi(^1T_{2u})|r|\Phi_0\rangle = (1/\sqrt{2})(\langle\Phi_0|r|\Phi_j^c\rangle - \langle\Phi_0|r|\Phi_k^b\rangle) = 0 \quad (34)$$

Here, the individual terms in the middle of eq 34 are nonzero, while those in eqs 31 and 32 are zero. Furthermore, since the integration for the transition dipole $\langle\phi_a|r|\phi_j\rangle$ includes the transition density term $\phi_a^*(r)\phi_j(r)$, this integral is expected to behave similarly to the above integrals K_{ja} and $(aj|ib)$.

Energy expressions for the excitations of $t_{1g} \rightarrow t_{2g}$, $t_{2g} \rightarrow t_{2g}$, $t_{2u} \rightarrow t_{2g}$, etc., may be derived similar to eqs 22−29 given for $t_{1u} \rightarrow t_{2g}$. The behavior of these splittings is analogous to that of the excited states of $t_{1u} \rightarrow t_{2g}$ shown in Figure 1. In the cases of $t_{1g} \rightarrow t_{2g}$ and $t_{2g} \rightarrow t_{2g}$, the elements corresponding to eqs 31−34 are always zero, and the four states are all dipole-forbidden. It is noted that these relationships for the energies and the transition dipole moments hold for octahedral molecules in general, regardless of the numbers of electrons involved, since they are derived using only group theory.

III. Application of FZOA to Octahedral MoF_6

In this study, we adopt MoF_6 as an example of an application of the FZOA method to octahedral metal complexes. We

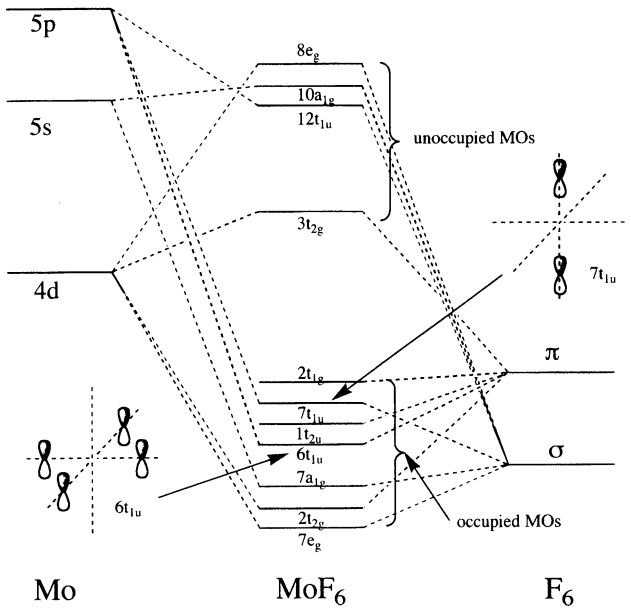

Figure 2. Schematic orbital correlation diagram for MoF_6 valence occupied MOs are σ-character MOs, $7a_{1g}$, $7e_g$, and $7t_{1u}$, and π-character MOs, $2t_{2g}$, $6t_{1u}$, $1t_{2u}$, and $2t_{1g}$, of the ligands. The unoccupied $3t_{2g}$ and $8e_g$ MOs are the 4d orbitals of Mo. Inserts show the $7t_{1u}$ and $6t_{1u}$ MOs.

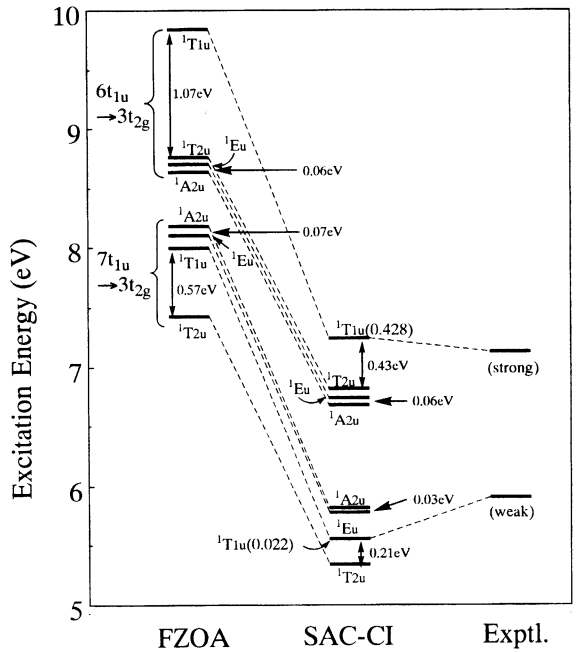

Figure 3. Energy levels of the $7t_{1u} \rightarrow 3t_{2g}$ and $6t_{1u} \rightarrow 3t_{2g}$ excitations of MoF_6 calculated by the SAC/SAC-CI method and the FZO approximation compared with the experimental peak positions of the UV spectrum.

calculated the ground and excited states of MoF_6 by the SAC/SAC-CI method.[15,16] The active space of the SAC/SAC-CI calculations includes the higher 18 occupied MOs and the lower 127 unoccupied MOs obtained by the HF method. For the SAC and SAC-CI calculations, energy thresholds of 3.0×10^{-5} and 4.0×10^{-5} hartree were used to select the linked configuration state functions, respectively.[51] The HF calculation was carried out using the program HONDO8.[52] The program system SAC85[53] was used for SAC-CI calculations.

The Gaussian basis set used for the molybdenum atom is the (43333/433/43)/[433321/4312/421] set of Huzinaga[54] augmented with two diffuse s (0.012 01 and 0.005 856) and four diffuse p (0.081, 0.026, 0.011 04, and 0.005 455) functions. For fluorine, we use the (73/7)/[721/61] set of Huzinaga[54] augmented with one p anion basis (0.074)[55] and two d polarization functions (3.559 and 0.682).[54]

Figure 2 shows the schematic orbital correlation diagram for MoF_6. Rydberg 6s, 6p, and higher orbitals are not shown. The valence occupied MOs consist of three σ-character MOs, $7a_{1g}$, $7e_g$, and $7t_{1u}$, and four π-character MOs, $2t_{2g}$, $6t_{1u}$, $1t_{2u}$, and $2t_{1g}$. The difference between the $7t_{1u}$ and $6t_{1u}$ MOs is illustrated in Figure 2. The b_{1u} element of the $7t_{1u}$ MOs has large amplitudes in the two ligands on the z axis, while that of the $6t_{1u}$ MOs in the four ligands on the xy plane. Since the $3t_{2g}$ and $8e_g$ MOs due to the 4d AOs of Mo are unoccupied, MoF_6 is called a d^0 complex. Strictly speaking, the 4d AOs of Mo contribute to the $7e_g$ and $2t_{2g}$ MOs, the 5s AO contributes to the $7a_{1g}$ MOs, and the 5p AOs contribute to the $6t_{1u}$ and $7t_{1u}$ MOs.

We examine here two excitations from t_{1u} to t_{2g} as an example, i.e., $7t_{1u} \rightarrow 3t_{2g}$ and $6t_{1u} \rightarrow 3t_{2g}$. All of the excited states of MoF_6 in the visible and UV regions will be discussed elsewhere.[49] Figure 3 shows the calculated excitation levels of the $7t_{1u} \rightarrow 3t_{2g}$ and $6t_{1u} \rightarrow 3t_{2g}$ excitations of MoF_6 by the SAC/SAC-CI method in comparison with the FZO approximation. Figure 3 also shows the peak position of the UV spectrum of MoF_6. On the basis of the SAC-CI results, we can assign the experimental peaks to the allowed transitions to the $^1T_{1u}$ states. The discrepancies between the theoretical and experimental results are 0.34 and 0.12 eV, respectively. The oscillator strength for the $6t_{1u} \rightarrow 3t_{2g}$ excitation is calculated to be 0.428, which is greater than that for the $7t_{1u} \rightarrow 3t_{2g}$ excitation (0.022). This trend agrees with the experimental intensities for the two peaks. We also calculated the $^1A_{2u}$, ^1E_u, and $^1T_{2u}$ states corresponding to the forbidden transitions. The ordering of these four states differs between the $7t_{1u} \rightarrow 3t_{2g}$ and $6t_{1u} \rightarrow 3t_{2g}$ excitations, i.e., $^1T_{2u} < {}^1T_{1u} < {}^1E_u < {}^1A_{2u}$ and $^1A_{2u} < {}^1E_u < {}^1T_{2u} < {}^1T_{1u}$, respectively.

These FZO calculations do not give quantitative results, since this treatment corresponds to the single-excitation (SE) CI calculation with a minimum active space [3 × 3]. In fact, the excitation energies are shifted upward by 1.95−2.59 eV, in comparison with the SAC-CI results shown in Figure 3. However, the ordering of the four states from the FZO approximation agrees with the SAC-CI results. Furthermore, in the FZO approximation, the energy splittings between the $^1T_{2u}$ and $^1T_{1u}$ states are greater than those between the ^1E_u and $^1A_{2u}$ states for both excitations, which also agrees with the SAC-CI results. Thus, the energy orderings and the splittings of the FZO approximation conserve various features of the accurate calculations that include the effects of electron correlations. Since the four states have the same term-multiplicity, the electron correlations for these states may be similar to each other. This agreement allows us to use the FZOA method to explain the complicated excited states of MoF_6. We can imagine that the present results are similar to those associated with the use of Hund's rule.

Table 1 shows the numerical data for the orbital energies and two-electron integrals in eqs 22−25. The absolute values of the Coulomb integrals are greater than those of the exchange and four-center integrals. The order of the $(ai|jb)$ and $(aj|ib)$ four-center integrals is the same as that of the exchange integrals. The relationship between $(^1A_{2u}, {}^1E_u)$ and $(^1T_{1u}, {}^1T_{2u})$ of the $7t_{1u} \rightarrow 3t_{2g}$ excitation is determined by the difference between the Coulomb integrals. On the other hand, the relationship between $(^1A_{2u}, {}^1E_u)$ and $(^1T_{1u}, {}^1T_{2u})$ of the $6t_{1u} \rightarrow 3t_{2g}$ excitation is determined by the difference between the exchange integrals, since the difference between J_{ia} and J_{ja} is small. The $3t_{2g}$ MOs are the d_{xy}, d_{zx}, and d_{yz} AOs of Mo, and the $7t_{1u}$ and $6t_{1u}$ MOs are the σ- and π-character MOs of the ligands, as mentioned above. For the $7t_{1u}$ and $3t_{2g}$ MOs, the J_{ia} and J_{ja} electron

TABLE 1: Numerical Data for the Orbital Energies, Coulomb, Exchange, and Four-Center Two-Electron Integrals in Eqs 22−25 for the $7t'_{1u} \rightarrow 3t_{2g}$ and 6t1u → 3t2g Excited States of MoF_6[a]

	A term			B term			C term		
	ϵ_i	ϵ_a	total	J_{ia} J_{ja}	K_{ia} K_{ja}	total	$(ai\|jb)$ $(aj\|ib)$	$(ab\|ij)$	total
				$7t_{1u} \rightarrow 3t_{2g}$					
$^1A_{2u}$	−18.7537	−3.1640	15.5897	7.5155	0.0260	−7.4635	0.0151	0.0046	0.0512
^1E_u	−18.7537	−3.1640	15.5897	7.5155	0.0260	−7.4635	0.0151	0.0046	−0.0257
$^1T_{1u}$	−18.7537	−3.1640	15.5897	8.3439	0.2327	−7.8785	0.1464	0.0046	0.2882
$^1T_{2u}$	−18.7537	−3.1640	15.5897	8.3439	0.2327	−7.8785	0.1464	0.0046	−0.2882
				$6t_{1u} \rightarrow 3t_{2g}$					
$^1A_{2u}$	−19.8194	−3.1640	16.6554	8.0803	0.0517	−7.9769	0.0298	0.0816	0.0440
^1E_u	−19.8194	−3.1640	16.6554	8.0803	0.0517	−7.9769	0.0298	0.0816	−0.0220
$^1T_{1u}$	−19.8194	−3.1640	16.6554	8.1323	0.3891	−7.3541	0.3101	0.0816	0.5386
$^1T_{2u}$	−19.8194	−3.1640	16.6554	8.1323	0.3891	−7.3541	0.3101	0.0816	−0.5386

[a] The terms A, B, and C are defined in eq 30.

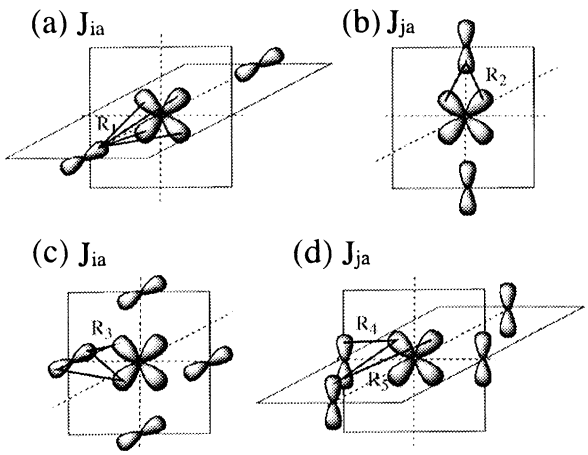

Figure 4. Analysis of the J_{ia} and J_{ja} electron repulsions. Parts a and b correspond to J_{ia} and J_{ja} between the $7t_{1u}$ and $3t_{2g}$ MOs, respectively. Parts c and d correspond to J_{ia} and J_{ja} between the $6t_{1u}$ and $3t_{2g}$ MOs, respectively. R_i (i = 1, 2, 3, 4, and 5) is defined qualitatively as the distance between the main amplitudes of the relevant electron densities.

repulsions are illustrated in Figure 4, parts a and b, respectively. The distance R_1 between the electron densities of $7t_{1u}$ and $3t_{2g}$ MOs in the J_{ia} integral is much smaller than the distance R_2 in the J_{ja} integral, which explains why one finds that $J_{ia} < J_{ja}$. For the $6t_{1u}$ and $3t_{2g}$ MOs, the J_{ia} and J_{ja} repulsions are illustrated in Figure 4, parts c and d, respectively. Although the relationship $R_4 > R_3 > R_5$ may exist for the distances in Figure 4, the differences among these distances are small and do not lead to any significant difference between J_{ia} and J_{ja}, as shown in Table 1.

The exchange integrals K_{ia} and K_{ja} include the transition densities $\phi_a^*(r)\phi_i(r)$ and $\phi_a^*(r)\phi_j(r)$, respectively. Since the ϕ_i MO with b_{1u} symmetry has a node on the xy plane, while the ϕ_a MO is mainly the d_{xy} AO of Mo, the overlap between the ϕ_i and ϕ_a MOs is always zero in the xy, yz, and zx planes for both the $6t_{1u} \rightarrow 3t_{2g}$ and $7t_{1u} \rightarrow 3t_{2g}$ excited states. On the other hand, the overlap between the ϕ_j and ϕ_a MOs is nonzero, since the ϕ_j MO with b_{2u} symmetry includes the p_y orbitals of the ligands. This explains why we find $K_{ia} < K_{ja}$. As illustrated in Figure 5a,c, the overlaps between the ϕ_j and ϕ_a MOs for the $7t_{1u} \rightarrow 3t_{2g}$ and $6t_{1u} \rightarrow 3t_{2g}$ excited states have main amplitudes near the y and x axes, respectively. Another difference between these states is that the signs of the neighboring amplitudes are different and the same in Figure 5, parts a and c, respectively. The amplitudes with different signs decrease the value of K_{ja} in the integration. Therefore, the value of K_{ja} for the $7t_{1u} \rightarrow 3t_{2g}$ excitation is smaller than that for the $6t_{1u} \rightarrow 3t_{2g}$ excitation.

Since the phases of the ϕ_j and ϕ_b MOs do not match as well as those of the ϕ_i and ϕ_a MOs, the $(ai|jb)$ four-center integrals are smaller than the $(aj|ib)$ four-center integrals. This difference

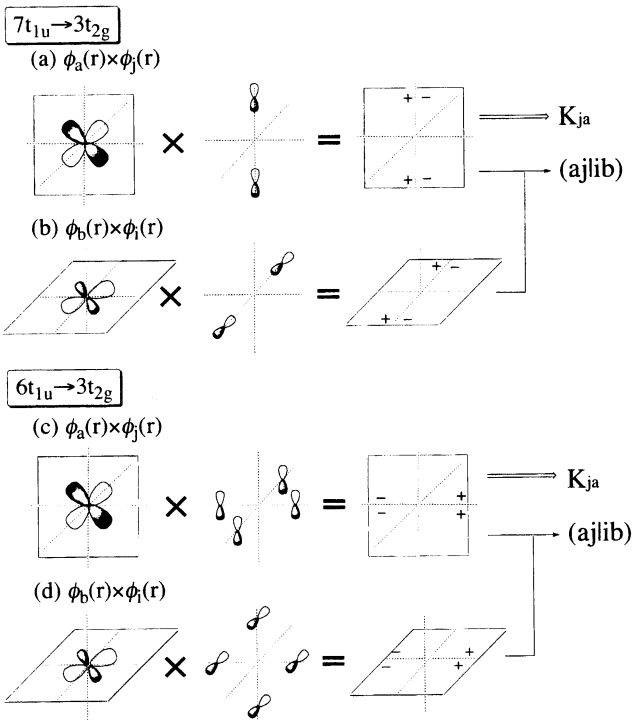

Figure 5. Analysis of the K_{ja} exchange integral and the $(aj|ib)$ four-center integrals. Parts a and b are the distribution of the transition density between the ϕ_j (b_{2u}) and ϕ_a (b_{1g}) MOs and that between ϕ_i (b_{1u}) and ϕ_b (b_{2g}) MOs, respectively, for the $7t_{1u} \rightarrow 3t_{2g}$ excited states. Figures c and d show the same distributions for the $6t_{1u} \rightarrow 3t_{2g}$ excited states.

leads to the larger energy splittings between the $^1T_{1u}$ and $^1T_{2u}$ states compared with the splittings between the $^1A_{2u}$ and ^1E_u states. For the $6t_{1u} \rightarrow 3t_{2g}$ and $7t_{1u} \rightarrow 3t_{2g}$ states, the different orderings of the $^1A_{2u}$ and ^1E_u states are due to the different sign of the C term in eq 30. As illustrated in Figure 5b,d, the overlaps between the ϕ_i and ϕ_b MOs for the $7t_{1u} \rightarrow 3t_{2g}$ and $6t_{1u} \rightarrow 3t_{2g}$ states have their maximal amplitudes near the z and x axes, respectively. Since the distance between the amplitude maxima of $\phi_a^*(r)\phi_j(r)$ and $\phi_i^*(r)\phi_b(r)$ is smaller for the $6t_{1u} \rightarrow 3t_{2g}$ state than that for the $7t_{1u} \rightarrow 3t_{2g}$ state, the former has a larger value of $(aj|ib)$. Therefore, the splitting between the $^1T_{1u}$ and $^1T_{2u}$ states of the $6t_{1u} \rightarrow 3t_{2g}$ state is greater than that of the $7t_{1u} \rightarrow 3t_{2g}$ state.

Due to the mismatch of the phases of the ϕ_a and ϕ_i MOs, the transition dipole moments of $\langle\phi_a|r|\phi_i\rangle$ are zero. On the other hand, the transition dipole moments of $\langle\phi_a|r|\phi_j\rangle$ have x elements. As a consequence, the order of the three integrals $\{K_{ia}, K_{ja}\}$, $\{(ai|jb), (aj|ib)\}$, and $\{\langle\phi_a|r|\phi_i\rangle, \langle\phi_a|r|\phi_j\rangle\}$ is similar in each case, since the transition density contributes equally to these integrals. On account of the different separations between the plus and

minus amplitudes of $\phi_a^*(r)\phi_j(r)$ in the x-axis direction, the transition dipole moment $\langle\phi_a|x|\phi_j\rangle$ of the $6t_{1u} \rightarrow 3t_{2g}$ state is greater than that of the $7t_{1u} \rightarrow 3t_{2g}$ state. This result shows that the intensity of the excitation from the π-character MO of the ligands to the d orbitals of the metal is greater than that from the σ-character MO of the ligands.

The present discussion gives a qualitative explanation for the ordering and the splitting of the four excited states with the $7t_{1u} \rightarrow 3t_{2g}$ and $6t_{1u} \rightarrow 3t_{2g}$ excitation nature. The energy splitting of the excited states calculated by the SAC-CI method is not determined solely by the simple B and C terms in eq 30. However, the analysis of these terms can provide a good explanation of the excited states of metal complexes. Since the analyses of the two-electron integrals in eqs 22−25 are mainly based on the symmetries and the bonding characters (σ or π) of the relevant MOs, the results of the present study can be applied to all octahedral metal complexes. Thus, the following relationships are established as general rules for the excited states of octahedral metal complexes:

(i) Ordering

$$^1T_{2u} < {}^1T_{1u} < ({}^1E_u < {}^1A_{2u}) \quad t_{1u}(\sigma) \rightarrow 3t_{2g}$$

$$({}^1A_{2u} < {}^1E_u) < {}^1T_{2u} < {}^1T_{1u} \quad t_{1u}(\pi) \rightarrow 3t_{2g}$$

(ii) Splitting

$$\Delta E(^1T_{1u}) - \Delta E(^1T_{2u}) \gg |\Delta E(^1A_{2u}) - \Delta E(^1E_u)| \quad t_{1u}(\sigma, \pi) \rightarrow 3t_{2g}$$

(iii) Intensity

$$I(^1T_{1u}; \pi) > I(^1T_{1u}; \sigma) \quad t_{1u}(\pi) \rightarrow 3t_{2g} \text{ vs } t_{1u}(\sigma) \rightarrow 3t_{2g}$$

where the parentheses in (i) indicate that the ordering of the ^1E_u and $^1A_{2u}$ states is uncertain because of the small splitting between them.

Finally, using the FZOA approach, we are able to predict the ordering and the splitting of triplet states within the $t_{1u}(\sigma) \rightarrow 3t_{2g}$ and $t_{1u}(\pi) \rightarrow 3t_{2g}$ excitations, which are not calculated for MoF_6 in the present study. The energy expressions of the triplet excitations in eqs 26−29 do not include the exchange integrals K_{ia} and K_{ja}, which lead to the difference in the ordering for the singlet excited states of the two excitation series. Likewise, they do not include the integrals $(ai|jb)$ and $(aj|ib)$, which produce the difference in splitting for the $\{^1T_{2u}, {}^1T_{1u}\}$ and $\{^1E_u, {}^1A_{2u}\}$ states. Therefore, the following relationships may be established for triplet states:

(iv) Ordering

$$^3T_{1u} < {}^3T_{2u} < {}^3A_{2u} < {}^3E_u \quad t_{1u}(\sigma, \pi) \rightarrow 3t_{2g}$$

(v) Splitting

$$\Delta E(^3T_{2u}) - \Delta E(^3T_{1u}) \leq \Delta E(^3E_u) - \Delta E(^3A_{2u}) \quad t_{1u}(\sigma, \pi) \rightarrow 3t_{2g}$$

$$\Delta E(^3T_{2u}) - \Delta E(^3T_{1u}) \ll \Delta E(^1T_{1u}) - \Delta E(^1T_{2u}) \quad \text{triplet vs singlet}$$

IV. Conclusion

In this report, we have proposed a frozen-orbital analysis (FZOA) for examining the excited states of metal complexes. This analysis provides an explanation of the ordering and the splitting of excited states due to the excitations between degenerate MOs.

We applied FZOA to the two $t_{1u} \rightarrow t_{2g}$ excitations of the octahedral MoF_6 complex. This excitation gives four states: $^1A_{2u}$, ^1E_u, $^1T_{1u}$, and $^1T_{2u}$. The energy levels of the ($^1A_{2u}$, ^1E_u) and ($^1T_{1u}$, $^1T_{2u}$) states are determined by the bonding characters of the t_{1u} MOs, i.e., σ and π. The energy splitting between the $^1T_{1u}$ and $^1T_{2u}$ states is larger than that between the $^1A_{2u}$ and ^1E_u states for both excitations. The difference in the transition dipole moment of the two excitations is explained by FZOA. Furthermore, the energy levels of the triplet states are predicted by FZOA.

It is noted that the splitting scheme obtained by FZOA does not depend on the numbers of electrons of molecules. Since the FZOA approach essentially uses the symmetries and the bonding characters of the relevant MOs, it can be applied to any systems of high symmetry and gives a general rule and concept for the ordering of the excited states. Apart from metal complexes, the method of FZOA has wider application, e.g., in understanding the energy levels of the excited states of organic molecules, metal clusters, or fullerenes. We are currently using FZOA to study several species under O_h, T_d, and I_h symmetries and also to investigate linear molecules.

Acknowledgment. The calculations were performed using computers at the Institute for Molecular Science. This study was supported in part by a Grant-in-Aid for Scientific Research from the Japanese Ministry of Education, Science, and Culture of Japan and by the New Energy and Industrial Technology Development Organization (NEDO).

References and Notes

(1) Lever, A. B. P. *Inorganic Electronic Spectroscopy*; Elsevier: Amsterdam, 1968.
(2) Teltow, J. *Z. Phys. Chem.* **1938**, *B40*, 397; **1939**, *43*, 198.
(3) Johnson, L. W.; McGlynn, S. P. *J. Chem. Phys.* **1971**, *55*, 2985; *Chem. Phys. Lett.* **1971**, *10*, 595. Johnson, L. W.; Hughes, E.; McGlynn, S. P. *J. Chem. Phys.* **1971**, *55*, 4476.
(4) Balzani, V.; Carasitti, V. *Photochemistry of Coordination Compounds*; Academic Press: New York, 1970.
(5) Adamson, A. W., Fleischauer, P. D., Eds. *Concepts of Inorganic Photochemistry*; Wiley-Interscience: New York, 1975.
(6) Geoffroy, G. L.; Wrighton, M. S. *Organometallic Photochemistry*; Academic Press: New York, 1979.
(7) Figgis, B. N. *Introduction to Ligand Fields*; Interscience: London, 1969.
(8) Ballhausen, C. J. *Introduction to Ligand Field Theory*; McGraw-Hill: New York, 1962.
(9) Jørgensen, C. K. *Modern Aspects of Ligand Field Theory*; North-Holland: Amsterdam, 1970.
(10) Jørgensen, C. K. *Absorption Spectra and Chemical Bonding in Complexes*; Pergamon Press: Oxford, U.K., 1962.
(11) Orgel, L. E. *J. Chem. Phys.* **1955**, *23*, 1004; *J. Chem. Soc.* **1952**, 4756; *Q. Rev., Chem. Soc.* **1952**, *8*, 422.
(12) Tanabe, Y.; Sugano, S. *J. Phys. Soc. Jpn.* **1954**, *9*, 753, 766.
(13) Jørgensen, C. K. *Mol. Phys* **1959**, *2*, 309; **1962**, *5*, 271; *Prog. Inorg. Chem.* **1971**, *12*, 101.
(14) Wolfsberg, M.; Helmholtz, L. *J. Chem. Phys.* **1952**, *20*, 837.
(15) Nakatsuji, H.; Hirao, K. *J. Chem. Phys.* **1978**, *68*, 2035.
(16) Nakatsuji, H. *Chem. Phys. Lett.* **1978**, *59*, 362; **1979**, *67*, 329, 334.
(17) Nakatsuji, H. *Acta Chim. Hung.* **1992**, *129*, 719.
(18) Nakatsuji, H.; Hirao, K. *Int. J. Quantum Chem.* **1981**, *20*, 1301.
(19) Nakatsuji, H.; Saito, S. *Int. J. Quantum Chem.* **1991**, *39*, 93.
(20) Nakai, H.; Ohmori, Y.; Nakatsuji, H. *J. Chem. Phys.* **1991**, *95*, 8287.
(21) Hasegawa, J.; Toyota, K.; Hada, M.; Nakai, H.; Nakatsuji, H. *Theor. Chim. Acta* **1995**, *92*, 351.
(22) Jitsuhiro, S.; Nakai, H.; Hada, M.; Nakatsuji, H. *J. Chem. Phys.* **1994**, *101*, 1029.
(23) Nakatsuji, H.; Saito, S. *J. Chem. Phys.* **1990**, *93*, 1865.
(24) Nakatsuji, H.; Ehara, M., Palmer, M. H.; Guest, M. F. *J. Chem. Phys.* **1992**, *87*, 2561.
(25) Nakatsuji, H.; Ehara, M. *J. Chem. Phys.* **1994**, *101*, 7658.
(26) Yasuda, K.; Nakatsuji, H. *J. Chem. Phys.* **1993**, *99*, 1945.

(27) Yasuda, K.; Kishimoto, N.; Nakatsuji, H. *J. Phys. Chem.* **1995**, *99*, 12501.
(28) Nakatsuji, H.; Hasegawa, J.; Hada, M. *J. Chem. Phys.* **1996**, *104*, 2321.
(29) Hasegawa, J.; Hada, M.; Nakatsuji, H. *Chem. Phys. Lett.* **1996**, *250*, 159.
(30) Nakatsuji, H.; Hasegawa, J.; Hada, M. *Chem. Phys. Lett.* **1996**, *250*, 379.
(31) Toyota, K.; Hasegawa, J.; Nakatsuji, H. *Chem. Phys. Lett.* **1996**, *250*, 437.
(32) Andersson, K.; Malmqvist, P.-Å.; Roos, B. O.; Sadlej, A. J.; Wolinski, K. *J. Phys. Chem.* **1990**, *94*, 5483.
(33) Andersson, K.; Malmqvist, P.-Å.; Roos, B. O. *J. Chem. Phys.* **1992**, *96*, 1218.
(34) Roos, B. O.; Fülscher, M. P.; Malmqvist, P.-Å.; Serrano-Andrés, P.-L.; Merchán, M. *Quantum Mechanical Electronic Structure Calculations with Chemical Accuracy*; Langhoff, S. R., Eds.; Kulter: Dordrecht, The Netherlands, 1994; Chapter 8.
(35) Andersson, K.; Roos, B. O. *Modern Electronic Structure Theory*; Yarkony, D. R., Eds.; World Scientific Publishing: New York, 1994; Vol. 1.
(36) Hund, F. *Z. Phys.* **1925**, *33*, 345.
(37) Messmer, R. P.; Briss, F. W. *J. Phys. Chem.* **1969**, *73*, 2085.
(38) Accad, Y.; Pekeris, C. L.; Schiff, B. *Phys. Rev.* **1971**, *A4*, 516.
(39) Katriel, J. *Theor. Chim. Acta* **1972**, *23*, 309.
(40) Kohl, D. A. *J. Chem. Phys.* **1972**, *56*, 4236.
(41) Boyd, R. J.; Coulson, C. A. *J. Phys.* **1973**, *B6*, 782.
(42) Colpa, J. P.; Islip, M. F. J. *Mol. Phys.* **1973**, *25*, 701. Colpa, J. P.; Thakkar, A. J.; Smith, V. H., Jr.; Randle, P. *Ibid.* **1975**, *29*, 1861.
(43) Killingbeck, J. *Mol. Phys.* **1973**, *25*, 455.
(44) Coulson, E. A. *J. Phys.* **1973**, *B6*, 2618. Coulson, E. A.; Coulson, C. A. *Ibid.* **1974**, *B7*, 1574. Coulson, E. A. *Ibid.* **1975**, *B8*, 1926.
(45) Shim, I.; Dahl, J. P. *Theor. Chim. Acta* **1978**, *48*, 165.
(46) Tatewaki, H.; Tanaka, K. *J. Chem. Phys.* **1974**, *60*, 601.
(47) Boyd, R. J. *Nature* **1984**, *310*, 480.
(48) Warner, J. W.; Berry, R. S. *Nature* **1985**, *313*, 160.
(49) Nakai, H.; Morita, H.; Tomasello, P.; Nakatsuji, H. Unpublished work.
(50) Nakai, H.; Morita, H.; Hanada, H.; Nakatsuji, H. Unpublished work.
(51) Nakatsuji, H. *Chem. Phys.* **1983**, *75*, 425.
(52) Dupuis, M.; Farazdel, A. *Program System HONDO8 from MOTECC-91*, 1991.
(53) Nakatsuji, H. *Program System for SAC and SAC-CI calculations*; Program Library No. 146 (Y4/SAC), Data Processing Center of Kyoto University, 1985; Program Library SAC85, No. 1396, Computer Center of the Institute for Molecular Science, 1981.
(54) Huzinaga, S.; Andzelm, J.; Klobukowski, M.; Radzio-Andzelm, E.; Sakai, Y.; Tatewaki, H. *Gaussian Basis Sets for Molecular Calculations*; Elsevier: New York, 1984.
(55) Dunning, T. H., Jr.; Hay, P. J. *Modern Theoretical Chemistry*; Schaeffer, H. F., III, Eds.; Plenum: New York, 1977; Vol. 3.

JP960310X